Volume 7 | Number 8 | 28 February 2015 | Pages 3321–3788

Nanoscale

www.rsc.org/nanoscale

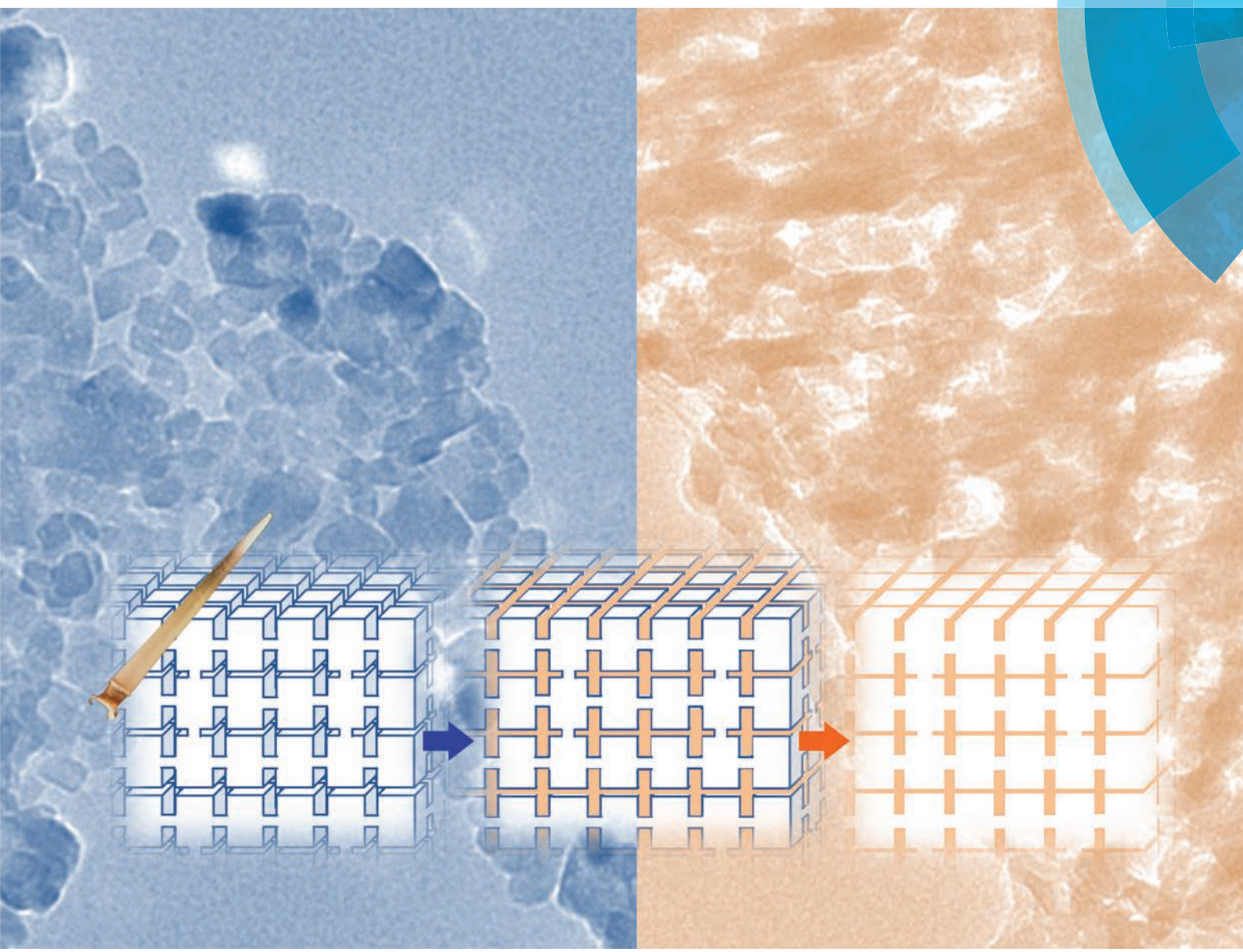

ISSN 2040-3364

ROYAL SOCIETY OF CHEMISTRY

PAPER

Yuya Oaki, Hiroaki Imai *et al.*

Incorporation of organic crystals into the interspace of oriented nanocrystals: morphologies and properties

NCNST

Nanoscale

PAPER

View Article Online
View Journal | View Issue

Cite this: *Nanoscale*, 2015, **7**, 3466

Incorporation of organic crystals into the interspace of oriented nanocrystals: morphologies and properties†

Yurika Munekawa, Yuya Oaki,* Kosuke Sato and Hiroaki Imai*

Received 12th September 2014,
Accepted 2nd December 2014

DOI: 10.1039/c4nr05317f

www.rsc.org/nanoscale

Oriented nanocrystals, as seen in biominerals, have both the macroscopic hierarchical morphologies and the nanoscale interspace among the unit crystals. Here we studied the incorporation effects of the specific interspace in the oriented nanocrystals on the morphologies, properties, and applications of organic crystals. Organic crystals, such as 9-vinylcarbazole (VCz), azobenzene (AB), and pyrene (PY), were introduced into the specific interspace of oriented nanocrystals from the melts. The morphologies and properties of the incorporated organic crystals were systematically studied in these model cases. The incorporation of the organic crystals provided the composites with the original oriented nanocrystals. The incorporated organic crystals formed the single-crystalline structures even in the nanoscale interspace. The melts of the organic compounds were crystallized and grown in the interspace of the original materials. The incorporated organic crystals showed the specific phase transition behavior. The freezing points of the organic crystals were raised by the incorporation into the nanospace while the melting points were not changed. The hierarchical morphologies of the organic crystals were obtained after the dissolution of the original materials. The hierarchical morphologies of the original materials were replicated to the organic crystals. The incorporated organic crystal was polymerized without deformation of the hierarchical morphologies. The hierarchical polymer can be applied to the donor material for the generation of a larger amount of the charge-transfer complex with the acceptor molecule than the commercial polymer microparticles. The present work shows the potential use of the nanoscale interspace generated in the oriented nanocrystals.

Introduction

Organized structures of oriented nanocrystals have attracted much interest in recent years.[1,2] The nanoscale interspace between the unit crystals can incorporate guest materials.[3,4] Here we incorporated a couple of organic crystals into the interspace of the oriented nanocrystal. The incorporation effects of the interspace on the morphologies and properties of the incorporated organic crystals were systematically studied for an improved understanding of the nanoscale interspace. Recent reports have shown a variety of the oriented nanocrystals, such as mesocrystals and bridged nanocrystals, found in biominerals and biomimetic materials.[5] Organization of nanocrystals as the building blocks generates a variety of hierarchical morphologies from the nanoscopic to the macroscopic scale. The syntheses, formation mechanisms, and applications of oriented nanocrystals have been widely studied in recent reports.[6–15] For example, oriented nanocrystals were applied to catalysts and electrode materials with improved performances.[12–14] In a review paper,[1g] Zhou and O'Brien indicated that the high performances are mainly ascribed to the contribution of the unit nanocrystals. Our recent challenge has been to exhibit the nature of the oriented nanocrystals as organized structures. We have studied the interspace of the unit crystals for incorporation of organic molecules.[3,4] The incorporation and polymerization of monomers in the nanospace direct the replication of the hierarchically organized morphologies from the original materials to the polymers.[4] The morphology replication is ascribed to not only the properties of each nanocrystal but also those of the organized structures. The organized structures of the oriented nanocrystals provide both the nanospace and the macroscopic morphologies. Our intention here is to study the incorporation effects of the nanospace on the morphologies, properties, and applications of organic crystals. The organic crystals were incorporated into the interspace of the oriented nanocrystals

Department of Applied Chemistry, Faculty of Science and Technology, Keio University, 3-14-1 Hiyoshi, Kohoku-ku, Yokohama 223-8522, Japan. E-mail: oakiyuya@applc.keio.ac.jp, hiroaki@applc.keio.ac.jp

†Electronic supplementary information (ESI) available. See DOI: 10.1039/c4nr05317f

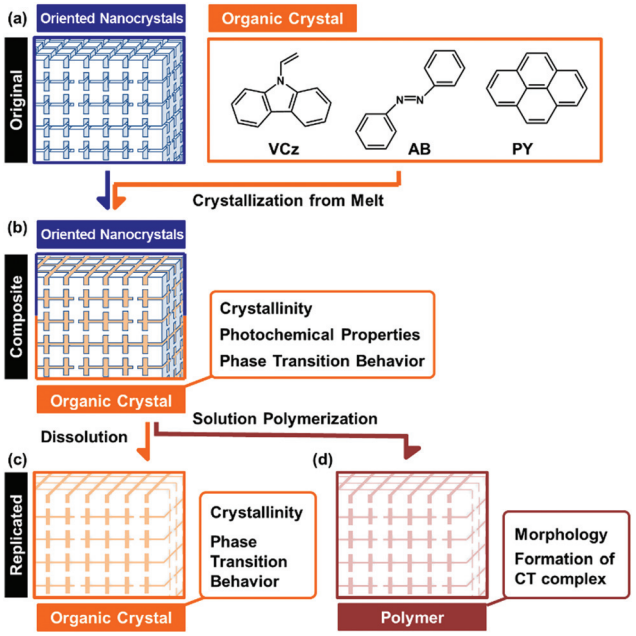

Fig. 1 Schematic illustration of the present study. (a) The original oriented nanocrystal and organic molecules for incorporation from the melts. (b) The composite after the incorporation. (c) The replicated organic crystals after the dissolution of the original material. (d) The polymerized material of an organic crystal after the dissolution of the original material.

from the melts (Fig. 1a and b). The hierarchical morphologies of the original materials were replicated to the organic crystals (Fig. 1b and c). Interestingly, the incorporated organic crystals formed the single crystalline structures even in the nanospace of the original materials. The specific phase-transition behavior was observed on the incorporated organic crystals. Materials with nanospace have been studied in recent decades, such as zeolites, porous materials, layered materials, and metal–organic frameworks.[16] A variety of applications has been developed using the nanospace, such as templates for morphogenesis,[17] adsorption sites, and reaction sites. Although the interspace of the oriented nanocrystals can incorporate the materials, further studies are required for an improved understanding of the interspace. Therefore, the present study shows the nature of the organic crystals incorporated into the interspace and an improved understanding of the nanospace.

Morphology control of organic materials has been studied in previous reports.[17–26] Designed molecules form the organized materials with the specific molecular orientation and morphology.[18–22] Morphologies of organic crystals are controlled by a variety of methods.[23–26] The polymer-mediated crystallization led to the formation of hierarchically organized organic crystals.[23–26] Morphologies of inorganic crystals are controlled by a variety of methods.[27] In contrast, it is not so easy to generate the hierarchical morphologies of organic crystals. In the present study, morphology control of the organic crystals was achieved using both the nanospace and hierarchical morphologies in the original materials. Here the melts of the organic crystals were introduced and crystallized in the nanospace of the oriented nanocrystals (Fig. 1a and b), although the viscosity of the melts was higher than that of the monomer liquid. The hierarchical morphologies of the original materials were replicated to the organic crystals (Fig. 1b and c). The present approach can be regarded as a generalizable approach to provide the hierarchical morphologies in the organic crystals.

In the present work, the organic crystals, such as 9-vinylcarbazole (VCz), azobenzene (AB), and pyrene (PY), were incorporated into the interspace of the oriented nanocrystals from their melts (Fig. 1). A sea urchin spine consisting of calcium carbonate ($CaCO_3$) with doping of magnesium ions was used as a model of oriented nanocrystals. A sea urchin spine is a suitable model because it has the complex hierarchical morphologies based on the oriented nanocrystals. Here the morphology of a sea urchin spine was successfully replicated to the organic crystals, such as VCz, AB and PY, through the formation of the composite states and the subsequent dissolution of the original materials. A similar morphology replication was achieved using the other original materials, such as the skeletal structure of a sea star and the synthetic vaterite oriented nanocrystals. Furthermore, the crystallinity, photochemical properties, and phase transition behavior were studied for the incorporated organic crystals in the composite state (Fig. 1b). Although the organic crystals were confined in the interspace of the nanocrystals, the crystallinity was not so remarkably lowered in the incorporated states. The incorporated organic crystals formed the single-crystalline structures. The melting (T_m) and freezing (T_f) points of the materials are generally lowered after incorporation into the nanospace. In contrast, the T_f of the incorporated organic crystals was raised, while the T_m was not changed. Polymerization of the incorporated VCz was achieved in the incorporated state without deformation of the morphology (Fig. 1d). The resulting PVCz formed a larger amount of the charge-transfer (CT) complex with 2,4,7-trinitro-9-fluorenone (TNF) than the commercial PVCz powder. In this way, the morphologies, properties, and applications were systematically studied on the organic crystals incorporated into the interspace of the oriented nanocrystals. The present study shows versatile potential of the nanoscale interspace among the unit crystals.

Results and discussion

Morphologies of the organic crystals

Organic crystals, such as VCz, AB, and PY, were incorporated into the $CaCO_3$ oriented nanocrystals from the melts (Fig. 1a). After the incorporation, the composites of the $CaCO_3$ oriented nanocrystals and the organic crystals were obtained (Fig. 1b). The dissolution of the original $CaCO_3$ led to the formation of organic crystals with the hierarchical morphologies (Fig. 1c). A sea urchin spine was immersed in the solution of sodium hypochlorite to remove the biological macromolecules. Then, the heat treatment was performed at 450 °C for 4 h to expand

the nanospace.[4] The original material was set with the powders of VCz, AB, and PY on a glass vessel at room temperature. The temperature of the samples was raised to 75 °C, 90 °C, and 180 °C by a heating stage for the incorporation of VCz, AB, and PY from their melts, respectively. The melting points of VCz, AB, and PY are known to be around 65 °C, 70 °C, and 150 °C, respectively. After incubation for 15–30 min, the excess amount of the melts was absorbed by a paper towel before cooling. The further detailed methods are described in the ESI.†

The original sea urchin spine shows a complex hierarchical structure (Fig. 2a–c).[5] The sponge morphology several tens of micrometer in size was observed on the cross-sectional image (Fig. 2a and b). The sponge morphology consisted of the oriented nanocrystals 20–50 nm in size (Fig. 2b and c). After the incorporation of VCz from the melt, the sponge morphology was preserved without infiltration of the micrometer-scale pores in the sponge with VCz (Fig. 2b and e). The original nanocrystals 20–50 nm in size were not clearly observed after the incorporation of VCz (Fig. 2e and f). Based on these observations, VCz was introduced not into the micrometer-scale pores of the sponge but into the nanospace in the skeletal body. The content of VCz in the composite was estimated to be 15 wt% by thermogravimetric (TG) analysis (Fig. S1 in the ESI†). The hierarchically replicated VCz was obtained after dissolution of the original $CaCO_3$ by hydrochloric acid (HCl) (Fig. 2g–i). The surface layer of the sponge skeletal body several micrometers in thickness was replicated to VCz (Fig. 2e and h). The inside part of the sponge skeletal body was not completely replicated to VCz because a sufficient amount of VCz was not introduced into the part. The replicated VCz sponge structure consisted of connected nanoparticles around 100 nm in size (Fig. 2h and i). When AB and Py were incorporated into the $CaCO_3$ original materials by the present method, the same morphology replication was achieved (Fig. S2 in the ESI†).

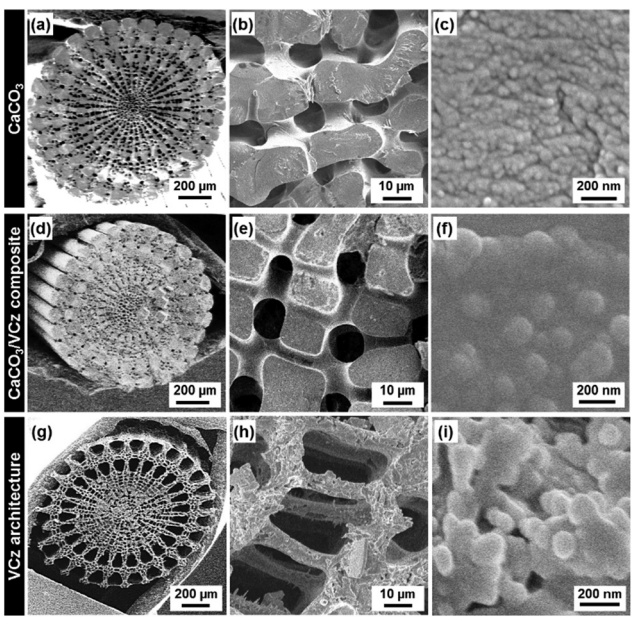

Fig. 2 Hierarchical morphology replication from a sea urchin spine as the original material to VCz as an organic crystal. (a–c) FESEM images of a sea urchin spine consisting of $CaCO_3$. (d–f) The composites of the $CaCO_3$ and VCz introduced from the melt. (g–i) VCz replicated architecture after the dissolution of the original material.

In our previous reports, the neat liquid and vapour of the monomers were incorporated into the interspace of the oriented nanocrystals.[4] In the current study, the same approach was applied to the incorporation of the organic crystals from their melts. Based on these facts, a variety of hydrophilic and hydrophobic liquids can be introduced into the nanoscale interspace. The results imply that the other organic molecules can be introduced from the liquid and vapour states, regardless of the hydrophilicity, hydrophobicity, and molecular size. The neat liquids of the monomers, such as pyrrole and thiophene derivatives, with low viscosity were incorporated into the nanospace throughout the macroscopic objects.[4c] Therefore, the whole hierarchical morphology of the original materials was replicated to the polymers. In contrast, the replication from the melts of the organic crystals was achieved on the surface layers of the micrometer-scale objects (Fig. 2e and h). The viscosity of these melts was higher than that of the monomer neat liquids. It is inferred that a sufficient amount of the melts is not introduced into the inside part of the micrometer-scale structures.

The original materials with the hierarchical morphologies based on the oriented nanocrystals were changed from a sea urchin spine to the other materials. A similar morphology replication was achieved by the exoskeleton of a sea star and the synthetic oriented nanocrystals of vaterite $CaCO_3$ (Fig. S3 in the ESI†).[15] The present approach can be applied to a variety of combinations of oriented nanocrystals and organic crystals for the morphogenesis.

Crystallinity of the incorporated organic crystals

The crystallinity of the incorporated organic crystals was studied by X-ray diffraction (XRD) and selected-area electron diffraction (SAED) (Fig. 3 and 4). If the size of the incorporated organic crystals is decreased by the confinement in the nanospace, the broadened peaks are observed on the XRD patterns. The commercial VCz crystals showed a number of peaks in the range of 2θ = 5–60° (profile (iv) in Fig. 3a). These peaks were assigned to those listed in the ICDD card (no. 00-033-1964). We focused on the strongest peak at 2θ = 10.2° corresponding to the (200) plane. The peak was observed on the composite containing 15 wt% of VCz (Fig. 3a). The half maximum at full-width (B) and the crystallite size based on Scherrer's equation (t) were estimated from the peaks of a commercial VCz powder, the composite with the incorporation of VCz into the $CaCO_3$ oriented nanocrystal, and the replicated architecture after the dissolution of the original $CaCO_3$ (Fig. 3b). As the reference, VCz powder was recrystallized with the same weight ratio of a commercial $CaCO_3$ crystal several micrometers in size by the same method. The same XRD analyses were performed on AB and PY samples (Table 1 and Fig. S4 in the

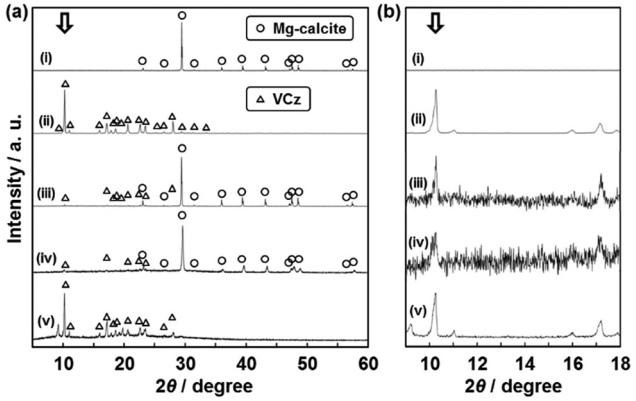

Fig. 3 XRD patterns (a) and their magnified ones (b) to study the crystallinity of VCz after incorporation into the oriented nanocrystals. Profiles (i)–(v) represent the following samples: (i) the exoskeleton of a sea urchin spine as the original material before the incorporation of VCz, (ii) a commercial VCz, (iii) the commercial VCz powder recrystallized with a commercial $CaCO_3$ powder, (iv) the composite after the incorporation of VCz into the original material, and (v) the replicated VCz architecture after the dissolution of the original material. Samples (iii) and (iv) contained the same amount of VCz, namely 15 wt%. The *B* and *t* were estimated from the peak at $2\theta = 10.2°$ denoted by white arrows (Table 1).

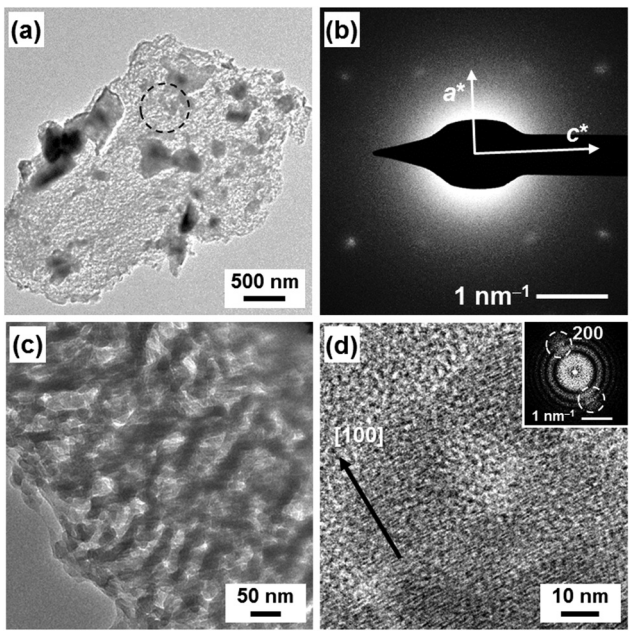

Fig. 4 FETEM analysis of the VCz replicated architecture. (a) FETEM image. (b) SAED pattern obtained from the circled area in panel (a). (c) The magnified FETEM image. (d) HRTEM image with its Fourier transform (inset).

ESI†). As shown in Table 1, the crystallite sizes were not decreased to single-nanometer size after recrystallization with $CaCO_3$ and incorporation into the oriented nanocrystals. When the commercial organic crystals and their mixtures with commercial $CaCO_3$ crystals were compared, the variations of *B* and *t* were within ±10% and ±30% respectively (Table 1). It means that the crystallinity is not so lowered after the recrystallization in the presence of $CaCO_3$ crystals. In the composite states, the decrease of *t* was a maximum of 51% after incorporation into the nanospace. However, the corresponding crystallite size was about 80 nm in size. The crystallinity of the incorporated organic crystals was not so lowered in the interspace of the oriented nanocrystals. These results imply that the incorporated organic crystals formed the single-crystalline structures within a certain length scale. Since the interspace of the oriented nanocrystals is not closed but continuously widespread in the original materials, the incorporated organic crystals can be grown to the specific sizes under the supercooled conditions.

Table 1 Crystallinity of the organic crystals, namely *B* and *t*, estimated from the XRD pattern

Sample	VCz		AB		PY	
Peak	$2\theta = 10.3°$		$2\theta = 17.3°$		$2\theta = 10.6°$	
Crystal plane	(200)		(102)		(001)	
$B/10^{-2}$° and *t*/nm	*B*	*t*	*B*	*t*	*B*	*t*
Commercial[a]	7.10	167	8.77	95.0	12.0	82.5
Mixture[b]	7.80	146	5.69	185	12.2	80.8
Composite[c]	12.1	81.6	4.32	220	13.7	70.1
Replica[d]	12.0	82.5	8.76	95.1	11.5	87.0

[a] Commercial powders of the organic crystals. [b] The mixture of the commercial $CaCO_3$ microcrystals and the organic crystals after the recrystallization. [c] The composite of the $CaCO_3$ oriented nanocrystal and the incorporated organic crystals. [d] The replicated architecture after the dissolution of the original materials. The detailed calculation method was described in the ESI.

The single-crystalline VCz architecture was observed by field-emission transmission electron microscopy (FETEM) (Fig. 4). In the replicated architectures, the crystallinity was not so changed from that of the composite state after dissolution of the original $CaCO_3$ (Fig. 3 and Table 1). The continuous nanoflakes of VCz around 50 nm were observed in the replicated architecture (Fig. 4a and c). The spot diffraction pattern assigned to VCz was obtained by SAED (Fig. 4b). A series of lattice fringes corresponding to the (200) plane of VCz was observed on the high-resolution TEM image (HRTEM) with the Fourier transform (Fig. 4d). These results suggest that the oriented VCz nanocrystals were formed in the replicated architecture. The XRD and SAED analyses suggest that the incorporated organic crystal formed single-crystalline structures. The nucleation of the incorporated organic crystals occurs on the surface of the original nanocrystals under the supercooled conditions. The growth of the organic crystals from the melts proceeds with the inclusion of the original nanocrystals in the continuous widespread nanospace. Therefore, the replicated materials form the single-crystalline structure in a certain scale.

Photochemical properties of the incorporated organic crystals

Photochemical properties, such as photoluminescence and photoisomerization, depend on the assembly state of mole-

cules. Here the photochemical properties of the incorporated AB and PY were the same as those of the bulk crystalline state (Fig. S5 in the ESI†). The photoisomerization behavior was not observed on the AB incorporated into the nanospace. When the composite was irradiated with the UV light at 365 nm, spectroscopic changes caused by the photoisomerization were not observed (Fig. S5 in the ESI†). If the photoisomerization reaction proceeds, the absorption peaks centered at 330 nm and 440 nm are decreased and increased respectively with irradiation of UV light.[28] The photoisomerization reaction was not observed on the bulk AB crystals. The results also supported that AB was incorporated as the crystalline state into the $CaCO_3$ oriented nanocrystals. The photoluminescence spectrum of the incorporated PY showed the same peaks as those corresponding to the bulk crystals (Fig. S5 in the ESI†). The broadened peak around 450 nm originating from the formation of the excimers was observed with UV light excitation at 330 nm. The same spectrum was obtained from the bulk PY crystals. If PY molecules are dispersed as the monomeric molecular state in the host materials, peaks around 400 nm can be observed on the spectrum.[29] The photoluminescence spectrum supported that the PY was incorporated as the crystalline state into the nanospace.

When AB and PY were introduced into the interspace of the oriented nanocrystals from the dilute solutions,[3] these organic compounds were dispersed in the nanospace as the monomeric molecular state. In the present work, these organic molecules were filled as the crystalline state in the nanospace. Therefore, the incorporated organic crystals showed the same photochemical properties as those of the bulk state. Based on the previous and the present studies, the assembly states of the organic molecules can be controlled in the interspace of the oriented nanocrystals by the introduction methods.

Thermal properties of the incorporated organic crystals

The T_m and T_f of VCz, AB, and PY were measured on the incorporated states in the nanospace using differential scanning calorimetry (DSC) (Fig. 5 and Table 2). In previous studies,[30,31] the T_m and T_f of the materials were generally lowered with confinement in nanoscale pores. In the present work, the T_m and T_f of the incorporated organic crystals into the oriented nanocrystal are expected to be lower than those of the bulk state. Interestingly, the T_f of the incorporated organic crystals was remarkably increased whereas the T_m was not changed by the incorporation into the nanospace (Fig. 5 and Table 2). The T_m and T_f were measured in the bulk organic crystals, the mixture of commercial $CaCO_3$ microcrystals and organic crystals and the mixture of $CaCO_3$ oriented nanocrystals and organic crystals. The heating and cooling of these samples were repeated by three cycles in the DSC measurement. The T_m and T_f of the VCz, AB, and PY were estimated from the onset temperature at the second cycles (Table 2). The first heating and cooling processes were regarded as the preparation of the composites of the $CaCO_3$ oriented nanocrystals and the organic crystals. In the other samples, the first cycle corresponded to the recrystallization of the organic compounds. As for VCz, the T_m was

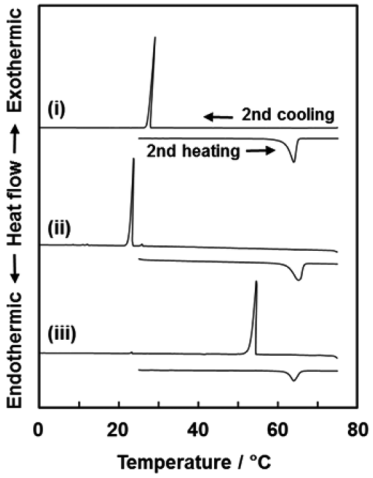

Fig. 5 DSC thermograms of a VCz commercial powder (i), the mixture of commercial $CaCO_3$ and VCz powders (ii), and the mixture of the $CaCO_3$ original material and a VCz commercial powder (iii). All the thermograms were obtained from the second heating and cooling processes. The onset temperature was used for the estimation of T_m and T_f in Table 2.

Table 2 T_m and T_f of the organic crystals in the different states[a]

Sample	VCz		AB		PY	
T_m, T_f/°C	T_m	T_f	T_m	T_f	T_m	T_f
Commercial[b]	62.0	26.7	67.1	24.6	149	121
Mixture[c]	62.7	22.7	67.2	42.6	148	130
Composite[d]	62.4	53.3	67.4	59.5	149	142

[a] The following samples were put in the DSC sample vessel. The onset temperature of the second cycles was adopted as the T_m and T_f listed in this table. [b] Commercial powders of the organic crystals. [c] The mixture of the commercial $CaCO_3$ microcrystals and the organic crystals after the recrystallization. [d] The composite of the $CaCO_3$ oriented nanocrystals and the incorporated organic crystals.

observed to be around 62 °C in the heating processes regardless of the samples (Fig. 5 and Table 2). In contrast, the T_f of the VCz in the oriented nanocrystal was raised from 24 °C to 53 °C in the cooling process. The same phase transition behavior, namely the rise of the T_f, was observed on the AB and PY (Table 2 and Fig. S6 in the ESI†).

The rise of the T_f is ascribed to the promotion of heterogeneous nucleation in the interspace of the oriented nanocrystal. The surface of the unit nanocrystals provides the heterogeneous nucleation sites in the melts of the organic compounds. A couple of previous studies showed the simultaneous rise of T_f and T_m.[32–34] The T_f of the polymers was raised when the inorganic nanoparticles were added into the polymer melts.[32] The presence of inorganic nanoparticles promoted the crystallization of the polymers through the specific interaction. The T_f of carbon tetrachloride was elevated by the confinement in graphitic carbon.[33] A calculation study also supported the experimental results.[34] When the interactions between the pore wall and the incorporated molecules were

stronger than those between the incorporated molecules, the T_f and T_m are raised by a decrease in the pore size. In the present work, only the T_f was raised by the incorporation into the nanoscale interspace. It is inferred that the sites for heterogeneous nucleation are provided by the surface of the unit nanocrystals. The crystal growth proceeds in the nanospace under the supercooled conditions. In contrast, the T_m was not changed by the incorporation into the nanospace. Since the organic crystals are grown to the specific size comparable to the bulk size, the melting behavior is not distinct from the bulk crystals. Therefore, the T_m is not influenced by the surface of the unit nanocrystals. The present phase transition behaviour is specific in the interspace of the oriented nanocrystals. A further study is needed for the understanding and application of the thermal properties.

Polymerization of VCz and the formation of the charge-transfer complex

PVCz was synthesized by the polymerization of the VCz in the composite state. In previous studies, PVCz was synthesized in the mesoporous materials and metal–organic frameworks.[35] In the present study, the hierarchical morphology of the PVCz was obtained after the dissolution of the original $CaCO_3$ material (Fig. 6). The CT complex was prepared by the immersion of the resulting PVCz in the toluene solution of TNF (Fig. 7). The PVCz hierarchical architectures formed a larger amount of the CT complex than commercial PVCz powder of several micrometers in size. The polymerization method was referred to previous reports.[36] The VCz incorporated into the oriented nanocrystal was immersed in a chloroform solution containing iron(III) chloride ($FeCl_3$). After the polymerization, the original $CaCO_3$ material was dissolved from the composite by HCl. The resulting PVCz showed similar hierarchical morphologies to the VCz (Fig. 2 and 6). A sponge structure consisting of nanoparticles 50 nm in size was obtained (Fig. 6a–d).

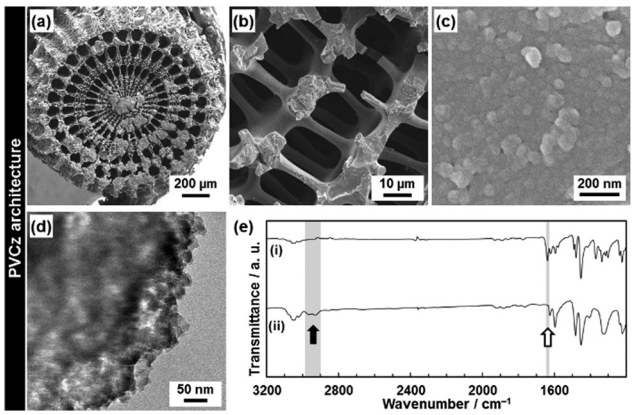

Fig. 6 Hierarchical architecture of PVCz after the dissolution of the original $CaCO_3$. (a–c) FESEM images after the dissolution of the original material, (d) FETEM image, (e) and FT-IR spectrum of the VCz architecture before (i) and after (ii) the polymerization reaction. In panel (e), the absorption around 2900–3000 cm^{-1} (black arrow) and 1630 cm^{-1} (white arrow) corresponds to the C–H stretching vibration and the C=C stretching vibration, respectively.

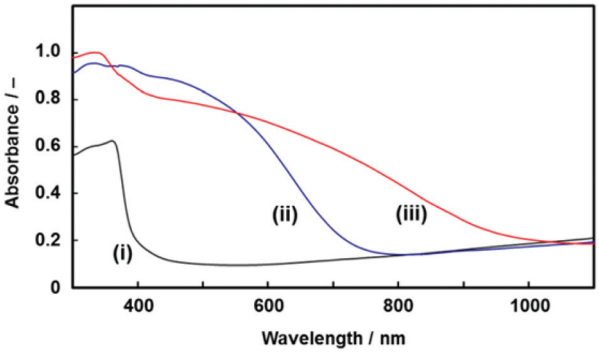

Fig. 7 UV-Vis absorption spectra of the resulting PVCz architecture (i), the CT complex of a commercial PVCz with TNF (ii), and the CT complex of the PVCz hierarchical architecture with TNF (iii).

The formation of PVCz was confirmed by the FT-IR spectrum (Fig. 6e).[37] A decrease and an increase in the absorptions corresponding to the C=C stretching vibration and the C–H stretching vibration, respectively, were observed after the polymerization. The crystallinity of VCz disappeared after the polymerization. When the VCz replicated architecture was used for the polymerization, the hierarchical morphologies were not kept after the dissolution of the original $CaCO_3$. The hierarchical morphology of PVCz was only obtained by the polymerization in the composite state. The interspace of the oriented nanocrystals and the framework of the macroscopic morphology contributes to the morphogenesis with the polymerization.

The CT complex was formed by the immersion of the resulting PVCz in a toluene solution of TNF. The PVCz had an absorption edge around 370 nm. A redshift of the absorption edge was observed by the immersion in the toluene solution of TNF (Fig. 7). Based on previous reports,[38] the redshift of the absorption spectrum is ascribed to the formation of the CT complex. The amount of the CT complex was estimated from the absorption peaks of the FT-IR spectra (Fig. S7 in the ESI†). About 11.2 mol% of the VCz units in the PVCz hierarchical architecture formed the CT complex with TNF, whereas 1.70 mol% of the VCz units in a commercial PVCz powder were used for the formation of the CT complex. Under the same conditions, the PVCz hierarchical architecture formed a 6.6 times higher amount of the CT complex than commercial PVCz powder. The specific surface area contributed to the formation of a larger amount of the CT complex. The morphology control of organic materials based on the present approach has potential use for the improvement of the properties.

Conclusions

Organic crystals, such as VCz, AB, and PY, were introduced into the interspace of the $CaCO_3$ oriented nanocrystals from the melts. The incorporation effects of the nanospace on the morphologies and properties of organic crystals incorporated were systematically studied. The original materials and the

incorporated organic crystals formed the composite. The hierarchical morphology of the organic crystals was obtained after the dissolution of the original materials. Although the melts of the organic crystals have high viscosities, the liquids were incorporated and crystallized in the nanospace. The crystallinity of the incorporated organic crystals was not lowered in the nanospace. The single-crystalline structure of the incorporated organic materials was formed in the composite states and the replicated architectures. The crystallization of the melts and the subsequent growth proceed in the nanospace with the inclusion of the original materials under supercooled conditions. A unique phase transition behavior was observed on the incorporated organic crystals in the nanospace. The incorporated organic crystals showed an elevation of T_f, whereas the T_m was not changed from the bulk state. It is inferred that the heterogeneous nucleation was promoted by the high specific surface area based on the unit nanocrystals. The incorporated organic crystal, namely VCz, was polymerized in the composite state. The hierarchical morphology of PVCz was obtained after the dissolution of the original material. The resulting PVCz formed a larger amount of the CT complex than the commercial PVCz powder. The present new results can be applied to a variety of combinations of oriented nanocrystals and organic materials. The morphologies and properties of organic crystals can be tuned by the incorporation into the nanoscale interspace of the hierarchically organized materials.

Acknowledgements

This work was partially supported by Grants-in-Aid for Scientific Research (no. 22107010) on Innovative Areas on "Fusion Materials: Creative Development of Materials and Exploration of Their Function through Molecular Control" (no. 2206) (H.I.) from the Ministry of Education, Culture, Sports, Science, and Technology and for Young Scientist (A, no. 22685022) (Y.O.) from the Japan Society for the Promotion of Science. We thank Prof. Y. Katayama for recording DSC thermograms.

Notes and references

1 (*a*) H. Cölfen and S. Mann, *Angew. Chem., Int. Ed.*, 2003, **42**, 2350; (*b*) H. Cölfen and M. Antonietti, *Angew. Chem., Int. Ed.*, 2005, **44**, 5576; (*c*) M. Niederberger and H. Cölfen, *Phys. Chem. Chem. Phys.*, 2006, **8**, 3271; (*d*) H. Imai, Y. Oaki and A. Kotachi, *Bull. Chem. Soc. Jpn.*, 2006, **79**, 1834; (*e*) L. Zhou and P. O'Brien, *Small*, 2008, **4**, 1566; (*f*) L. Zhou and P. O'Brien, *J. Phys. Chem. Lett.*, 2012, **3**, 620; (*g*) Y. Oaki and H. Imai, *SPR Nanosci.*, 2013, **1**, 1.

2 H. Cölfen and M. Antonietti, *Mesocrystals and Nonclassical Crystallization*, John Wiley & Sons, 2008.

3 (*a*) Y. Oaki and H. Imai, *Angew. Chem., Int. Ed.*, 2005, **44**, 6571; (*b*) Y. Oaki and H. Imai, *Bull. Chem. Soc. Jpn.*, 2009, **82**, 613.

4 (*a*) Y. Oaki, M. Kijima and H. Imai, *J. Am. Chem. Soc.*, 2011, **133**, 8594; (*b*) M. Kijima, Y. Oaki, Y. Munekawa and H. Imai, *Chem. – Eur. J.*, 2013, **19**, 2284; (*c*) Y. Munekawa, Y. Oaki and H. Imai, *Langmuir*, 2014, **30**, 3236; (*d*) R. Muramatsu, Y. Oaki, K. Kuwabara, K. Hayashi and H. Imai, *Chem. Commun.*, 2014, **50**, 11840.

5 (*a*) Y. Oaki, A. Kotachi, T. Miura and H. Imai, *Adv. Funct. Mater.*, 2006, **16**, 1633; (*b*) Y. Oaki and H. Imai, *Small*, 2006, **2**, 66.

6 S. H. Yu, M. Antonietti, H. Cölfen and J. Hartmann, *Nano Lett.*, 2003, **3**, 379.

7 (*a*) A. Sugawara, T. Nishimura, Y. Yamamoto, H. Inoue, H. Nagasawa and T. Kato, *Angew. Chem., Int. Ed.*, 2006, **45**, 2876; (*b*) T. Nishimura, T. Ito, Y. Yamamoto, M. Yoshio and T. Kato, *Angew. Chem., Int. Ed.*, 2008, **47**, 2800.

8 (*a*) Y. Oaki and H. Imai, *Adv. Funct. Mater.*, 2005, **15**, 1407; (*b*) Y. Oaki and H. Imai, *Chem. Commun.*, 2005, 6011.

9 L. Zhou, D. S. Boyle and P. O'Brien, *J. Am. Chem. Soc.*, 2007, **130**, 1309.

10 M. Kijima, Y. Oaki and H. Imai, *Chem. – Eur. J.*, 2011, **17**, 2828.

11 Y. Oaki, N. Yagita and H. Imai, *Chem. – Eur. J.*, 2012, **18**, 110.

12 I. Bilecka, A. Hintennach, I. Djerdj, P. Novák and M. Niederberger, *J. Mater. Chem.*, 2009, **19**, 5125.

13 J. Ye, W. Liu, J. Cai, S. Chen, X. Zhao, H. Zhou and L. Qi, *J. Am. Chem. Soc.*, 2011, **133**, 933.

14 F. Dang, T. Hoshino, Y. Oaki, E. Hosono, H. Zhou and H. Imai, *Nanoscale*, 2013, **5**, 2352.

15 H. Imai, N. Tochimoto, Y. Nishino, Y. Takezawa and Y. Oaki, *Cryst. Growth Des.*, 2012, **12**, 876.

16 (*a*) M. Ogawa and K. Kuroda, *Bull. Chem. Soc. Jpn.*, 1997, **70**, 2593; (*b*) B. J. Scott, G. Wrinsberger and G. D. Stacky, *Chem. Mater.*, 2001, **13**, 3140; (*c*) Y. Wan, H. Yang and D. Zhao, *Acc. Chem. Res.*, 2006, **39**, 423; (*d*) Y. Yamauchi and K. Kuroda, *Chem. – Asian J.*, 2008, **3**, 664; (*e*) T. Kimura and K. Kuroda, *Adv. Funct. Mater.*, 2009, **19**, 511; (*f*) N. Mizoshita, T. Tani and S. Inagaki, *Chem. Soc. Rev.*, 2011, **40**, 789; (*g*) S. Horike, S. Shimomura and S. Kitagawa, *Nat. Chem.*, 2009, **1**, 695; (*h*) T. Uemura, N. Yanai and S. Kitagawa, *Chem. Soc. Rev.*, 2009, **38**, 1228.

17 (*a*) E. Ruiz-Hitzky, *Adv. Mater.*, 1993, **5**, 334; (*b*) T. Tajima and T. Aida, *Chem. Commun.*, 2000, 2399; (*c*) R. A. Caruso and M. Antonietti, *Chem. Mater.*, 2001, **13**, 3272; (*d*) H. P. Hentze and M. Antonietti, *Curr. Opin. Solid State Mater. Sci.*, 2001, **5**, 343; (*e*) D. J. Cardin, *Adv. Mater.*, 2002, **14**, 553.

18 K. J. C. van Bommel, A. Friggeri and S. Shinkai, *Angew. Chem., Int. Ed.*, 2003, **42**, 980.

19 (*a*) T. Kato, *Science*, 2002, **295**, 2414; (*b*) T. Kato, N. Mizoshita and K. Kishimoto, *Angew. Chem., Int. Ed.*, 2006, **45**, 38; (*c*) T. Kato, T. Yasuda, Y. Kamikawa and M. Yoshio, *Chem. Commun.*, 2009, 729; (*d*) T. Ichikawa, M. Yoshio, S. Taguchi, J. Kagimoto, H. Ohno and T. Kato, *Chem. Sci.*, 2012, **3**, 2001.

20 A. R. Murphy and J. M. J. Fréchet, *Chem. Rev.*, 2007, **107**, 1066.
21 L. C. Palmer and S. I. Stupp, *Acc. Chem. Res.*, 2008, **41**, 1674.
22 S. J. Holder and N. A. J. M. Sommerdijk, *Polym. Chem.*, 2011, **2**, 1018.
23 (*a*) H. S. Nalwa, H. Kasai, S. Okada, H. Oikawa, H. Matsuda, A. Kakuta, A. Mukoh and H. Nakanishi, *Adv. Mater.*, 1993, **5**, 758; (*b*) D. Horn and J. Rieger, *Angew. Chem., Int. Ed.*, 2001, **40**, 4330; (*c*) Y. S. Zhao, H. Fu, A. Peng, Y. Ma, D. Xiao and J. Yao, *Adv. Mater.*, 2008, **20**, 2859; (*d*) R. Li, W. Hu, Y. Liu and D. Zhu, *Acc. Chem. Res.*, 2010, **43**, 529.
24 (*a*) H. P. Cong and S. H. Yu, *Chem. – Eur. J.*, 2007, **13**, 1533; (*b*) H. P. Cong and S. H. Yu, *Adv. Funct. Mater.*, 2008, **18**, 195.
25 (*a*) Y. Ma, G. Mehltretter, C. Plüg, N. Rademacher, M. U. Schmidt and H. Cölfen, *Adv. Funct. Mater.*, 2009, **19**, 2095; (*b*) Y. Jiang, H. Gong, D. Volkmer, L. Gower and H. Colfen, *Adv. Mater.*, 2011, **23**, 3548.
26 M. Huang, U. Schilde, M. Kumke, M. Antonietti and H. Cölfen, *J. Am. Chem. Soc.*, 2010, **132**, 3700.
27 (*a*) S. Mann, *Nature*, 1993, **365**, 499; (*b*) T. Kato, *Adv. Mater.*, 2000, **12**, 1543; (*c*) S. H. Yu and H. Cölfen, *J. Mater. Chem.*, 2004, **14**, 2124; (*d*) A.-W. Xu, Y. Ma and H. Cölfen, *J. Mater. Chem.*, 2007, **17**, 415; (*e*) F. C. Meldrum and H. Cölfen, *Chem. Rev.*, 2008, **108**, 4332; (*f*) N. A. J. M. Sommerdijk and G. de With, *Chem. Rev.*, 2008, **108**, 4499; (*g*) L. B. Gower, *Chem. Rev.*, 2008, **108**, 4551; (*h*) T. Kato, T. Sakamoto and T. Nishimura, *MRS Bull.*, 2010, **35**, 127; (*i*) H. Imai and Y. Oaki, *MRS Bull.*, 2010, **35**, 138.
28 G. S. Kumar and D. C. Neckers, *Chem. Rev.*, 1989, **89**, 1915.
29 T. Förster, *Angew. Chem., Int. Ed. Engl.*, 1969, **8**, 333.
30 (*a*) H. K. Christenson, *J. Phys.: Condens. Matter*, 2001, **13**, R95; (*b*) C. A. Simionesco, B. Coasne, G. Dosseh, G. Dudziak, K. E. Gubbins, R. Radhakrishnan and M. Sliwinska-Bartkowiak, *J. Phys.: Condens. Matter*, 2006, **18**, R15.
31 (*a*) C. L. Jackson and G. B. McKenna, *J. Chem. Phys.*, 1990, **93**, 9002; (*b*) J. C. van Miltenburg and J. P. van der Eerden, *J. Cryst. Growth*, 1993, **128**, 1143; (*c*) A. Schreiber, I. Ketelsen and G. H. Findenegg, *Phys. Chem. Chem. Phys.*, 2001, **3**, 1185; (*d*) G. Dosseh, Y. Xia and C. Alba-Simionesco, *J. Phys. Chem. B*, 2003, **107**, 6445.
32 (*a*) G. Z. Papageorgiou, D. S. Achilias, D. N. Bikiaris and G. P. Karayannidis, *Thermochim. Acta*, 2005, **427**, 117; (*b*) P. Maiti, P. H. Nam, M. Okamoto, N. Hasegawa and A. Usuki, *Macromolecules*, 2002, **35**, 2042; (*c*) P. Maiti and M. Okamoto, *Macromol. Mater. Eng.*, 2003, **288**, 440; (*d*) S. Zhang, A. Zhu and S. Dai, *J. Appl. Polym. Sci.*, 2011, **121**, 3007; (*e*) Z. Peng and D. Chen, *J. Polym. Sci., Part A: Polym. Phys.*, 2006, **44**, 534.
33 K. Kaneko, A. Watanabe, T. Iiyama, R. Radhakrishan and K. E. Gubbins, *J. Phys. Chem. B*, 1999, **103**, 7061.
34 M. Miyahara and K. E. Gubbins, *J. Chem. Phys.*, 1997, **106**, 2865.
35 (*a*) S. Spange, A. Gräser, H. Müller, Y. Zimmermann, P. Rehak, C. Jäger, H. Fuess and C. Baehtz, *Chem. Mater.*, 2001, **13**, 3698; (*b*) T. Uemura, N. Uchida, A. Asano, A. Saeki, S. Seki, M. Tsujimoto, S. Isoda and S. Kitagawa, *J. Am. Chem. Soc.*, 2012, **134**, 8360.
36 (*a*) D. B. Romero, M. Schaer, M. Leclerc, D. Adès, A. Siover and L. Zuppiroli, *Synth. Met.*, 1996, **80**, 271; (*b*) P. X. Thinh, C. Basavaraja, W. J. Kim and D. S. Huh, *Polym. Compos.*, 2011, **32**, 1772; (*c*) C. Bsavaraja, W. J. Kim, D. G. Kim and D. S. Huh, *Polym. Compos.*, 2011, **32**, 1077.
37 M. Sacak, U. Akbulut, C. Cheng and D. N. Batchelder, *Polymer*, 1994, **35**, 2495.
38 (*a*) B. Andre, R. Lever and J. Y. Moisan, *Chem. Phys.*, 1989, **137**, 281; (*b*) I. Glowacki, J. Jung and J. Ulański, *Synth. Met.*, 2000, **109**, 143; (*c*) J. Jung, I. Glowacki and J. Ulański, *J. Chem. Phys.*, 1999, **110**, 7000.